The Fourth IEEE RAS/EMBS International Conference
on Biomedical Robotics and Biomechatronics
Roma, Italy. June 24-27, 2012

Observations of Three-Dimensional Needle Deflection during Insertion into Soft Tissue

Alex Jahya, Ferdinand van der Heijden and Sarthak Misra

***Abstract*— Accurate needle placement is important during percutaneous needle insertion procedures such as biopsy and brachytherapy. However, needle-tissue interactions may cause the needle to deviate from its intended path. In this paper, we have investigated the effects of insertion velocity, tip bevel angle and insertion profile on needle deflection in three-dimensional space (in-plane and out-of-plane). Experiments are done using soft-tissue simulant and chicken liver. The needle tip is tracked during insertion using stereoscopic cameras and an electromagnetic tracker. Experimental results show that the in-plane and out-of-plane deflection decreases, as insertion velocity increases. Varying the bevel angle from 30° to 60° is shown to decrease the in-plane deflection, and increase the out-of-plane deflection. The addition of rotational motion during continuous linear insertion decreases both the in-plane and out-of-plane deflection. Tapping during insertion does not produce significant reduction in the in-plane or out-of-plane deflection. An increase in the insertion velocity from 10 mm/s to 300 mm/s during insertion into chicken liver results in the decrease and increase in the in-plane and out-of-plane deflection, respectively. A monotonic increase in the out-of-plane deflection as insertion velocity increases is probably caused by the needle slipping while penetrating the outer capsule of the liver. The results of this study can be used to develop an accurate model of needle-tissue interactions.**

I. Introduction

The most frequent and common methods to detect and treat cancer (e.g., in prostate, kidney and liver) are biopsy and brachytherapy, respectively [1],[2]. Both procedures involve percutaneous needle insertion where accurate tip placement is important for successful diagnosis and treatment. Yet, this is quite hard to achieve. Needle deflection and tissue deformation occur during needle insertion into soft and inhomogeneous tissue, causing the needle to deviate from its intended path [3],[4]. An example of a bevel-tip needle deviating from its path due to bending is shown in Fig. 1.

During insertion, the needle mainly deflects in the plane perpendicular to the bevel face (yz-plane) (Fig. 1). However, even a slight change in the bevel orientation due to needle bending results in the deflection along the xz-plane [5]. Tip deflection in the yz- and xz-plane are defined as in-plane and out-of-plane deflection, respectively.

Past work has shown that in-plane deflection is influenced by several parameters. Okamura *et al.* and Kataoka *et al.* studied the effects of tip geometry and soft-tissue elastic properties on tip deflection [6],[7]. Moreover, Abolhassani *et al.* showed that needle rotation and insertion velocity affected tip deflection [8]. Wan *et al.* showed that both continuous and 180° rotation at half of needle insertion distance reduced tip deflection [9]. Albohassani *et al.* and Wan *et al.* used bevel-tip needles in their experiments. Moreover, Minhas *et al.* showed that the curvature of needle trajectory can be controlled by incorporating duty-cycle spinning, resulting in the decrease in tip deflection [10].

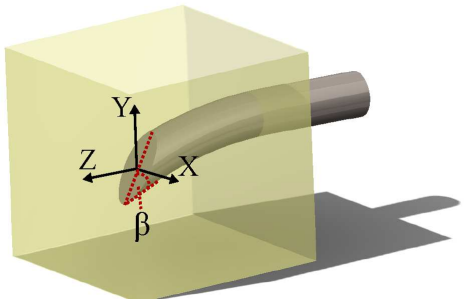

Fig. 1. A sketch of a needle bending due to tip asymmetry during insertion into soft-tissue simulant. Axis convention is shown in the figure. β is the bevel angle. The in-plane and out-of-plane deflection plane are yz- and xz-plane, respectively. Needle insertion is along the z-axis.

Furthermore, various *in vitro* studies have been done to investigate the influence of insertion distance, needle diameter and tip force on tip deflection. Kataoka *et al.* used a bi-plane X-ray imaging system to determine tip deflection in two dimensions [11]. Wan *et al.* performed experiments using bevel-tipped brachytherapy needles. They observed that the tip deflection was up to 2.8 mm for an insertion distance of 60 mm [5]. Hochman and Friedman experimented with various sizes of biopsy needles (25G, 27G and 30G). They showed that tip deflection of these needles ranged from 0.7 mm to 5 mm, and the largest deflection was noted for the 30G needle [12]. Lastly, Webster *et al.* performed needle insertion into a simulated muscle ballistic test media [13]. Their results showed that the increase in bevel angle reduced tip deflection. Moreover, they showed that the variation in insertion velocity (0.5 cm/s to 2.5 cm/s) produced no significant effect on tip deflection.

However, our literature review shows that there is a lack of data on the effects of system parameters on three-dimensional (3D) needle tip deflection. i.e., both in-plane and out-of-plane deflection. These parameters include insertion velocity, bevel angle, gel elasticity and insertion profile. During the percutaneous procedures, the needle tip has to be navigated in 3D space, away from the critical

The authors are affiliated with MIRA – Institute for Biomedical Technology and Technical Medicine, University of Twente, The Netherlands.
Email : {a.jahya, f.vanderheijden, s.misra}@utwente.nl

This research is supported by funds from the Dutch Ministry of Economic Affairs and the Province of Overijssel, within the Pieken in de Delta (PIDON) Initiative, Project MIRIAM (*Minimally Invasive Robotics In An MRI Environment*).

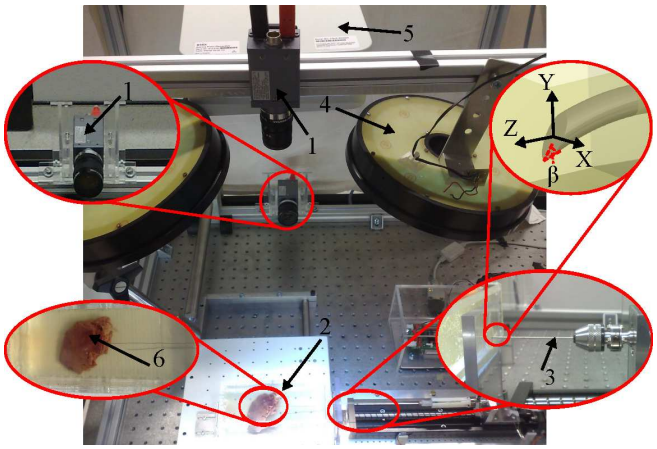

(a)

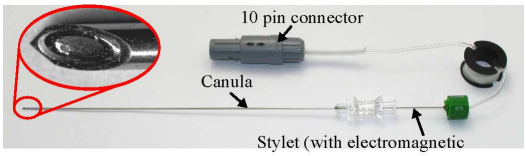

(b)

Fig. 2. (a) Two degree-of-freedom needle insertion setup used in the experiment. 1: Camera, 2: Gelatin mixture, 3: Needle, 4: Lighting, 5: Electromagnetic (EM) field generator and 6: Chicken liver. (b) 21G Chiba-tip EM-compatible needle. The needle consists of two parts, a stylet and a 21G outer cannula. A five degree-of-freedom EM sensor is embedded in the stylet at a distance of approximately 8 mm from the needle tip.

structures such as nerve bundles or blood vessels. For a conclusive biopsy and successful treatment, the tip has to be positioned within a spherical radius of 2.5 mm from the suspected lesion [14].

Moreover, accurate needle tip positioning in 3D space can further reduce the amount of radioactive dosage needed to treat the suspected lesion. Misplacements of the needle tip during the percutaneous procedures often leads to complications such as high radioactive dose loads and bleeding [15], [16]. In the prostate-related procedures, these complications often occur due to small size of the prostate (approximately 40 mm × 20 mm × 30 mm) [17]. Nevertheless, similar complications can also occur in any other organ. Since needle deflection has to be controlled in 3D space, rather just in two-dimensional (2D) space, out-of-plane deflection needs to be taken into account.

The goal of our study is to investigate the effects of insertion velocity, bevel angle and insertion profile on 3D (in-plane and out-of-plane) needle tip deflection. The experiments are performed using both soft-tissue simulant and soft tissue. In this study, chicken liver is used as the soft tissue.

The novel aspect of this study is that we investigate the effects of the system parameters on 3D needle tip deflection. A vision- and an electromagnetic (EM)-based system tracks the tip during needle insertion into transparent soft-tissue simulant and non-transparent chicken liver, respectively. The accuracy of the EM-based system is confirmed using the vision-based system, and the results are also presented in this study.

This paper is organized as follows: The experimental setup and methods are presented in Section II. Section III discusses the algorithms used for 2D needle tip tracking, and 3D needle tip location reconstruction. The experimental results are given in Section IV. Section V concludes with discussion and directions for future work.

II. Experimental Setup and Methods

A. System Description

The experimental setup and EM-compatible needle are presented in Fig. 2. Fig. 2(a) shows a two degree-of-freedom (DOF) needle insertion device designed to observe 3D needle tip deflection. The DOFs are translation along and rotation about the z-axis. In order to produce a translational motion, a Misumi translation stage (type LX3010) (MISUMI Group Inc. Tokyo, Japan), and a Maxon Motor (type RE25, with GP26B gearhead and HEDL5540 encoder, transmission ratio 4.4:1) (Maxon Motor, Sachseln, Switzerland) are used. Encoder resolution of HEDL5540 is 500 counts-per-turn (CPT), and the maximum achievable translational speed is 300 mm/s. The rotational motion is accomplished by another servomotor (Maxon Motor, type ECMax22 with Type M MR encoder). Encoder resolution of Type M MR is 512 CPT, and the maximum motor no load speed is 12400 revolutions-per-minute. Two Elmo Whistle 2.5/60 Digital Servo Drive (Elmo Motion Control Ltd, Petach-Tikva, Israel) control both motors.

Tracking of the needle tip is done using stereoscopic cameras and an Aurora EM system (Chiba-tip EM-compatible biopsy needle (Fig. 2(b)), and EM field generator (Item #5 in Fig. 2(a))) (Northern Digital Inc., Waterloo, Canada). Needle insertion into transparent soft-tissue simulant is tracked using the stereoscopic cameras, while *in vitro* insertion into the chicken liver is done using the Aurora EM system. The Aurora EM system allows tracking of the needle tip during insertion into non-transparent soft tissue.

Insertion into the soft-tissue simulant is recorded at 30 frames-per-second via two Sony XCD-SX90 charge-coupled device (CCD) FireWire cameras (Sony Corporation, Tokyo, Japan). The cameras (Item #1 in Fig. 2(a)) are located at 450 mm above the xz-plane (camera 1), and at 400 mm from the yz-plane (camera 2). The EM field generator is located at 500 mm above the xz-plane.

B. Methods

The first phase of our experiments is to investigate the effects of bevel angle, insertion velocity, gel elasticity and insertion profile on tip deflection. A gelatin mixture is used as the soft-tissue simulant. The compositional percentage of gelatin in the mixture is varied to produce two types of simulants with different elasticities, $E_1 = 8.7$ kPa and $E_2 = 35.5$ kPa. Elasticities of the simulants are determined at room temperature (22 °C) using dynamic mechanical analysis (Anton Paar, Gentbrugge, Belgium) [18]. Identical preparation procedures are also used for all experiments in

order to ensure consistent properties of the gelatin mixture except for elasticity.

All needles are of 1 mm diameter (ϕ) solid stainless-steel wires with bevel angles (β) of 30°, 45° and 60°. The insertion distance is kept constant at 100 mm. The experimental studies (Experiments #1 to #5) are tabulated in Table 1. Each experiment is repeated three times, and the result presented is the average of three data points.

Furthermore, insertion profiles investigated are continuous, rotation and tapping motion. Continuous insertion is done at insertion speed of 10 mm/s, 20 mm/s, 50 mm/s and 300 mm/s, respectively [19]. Rotational motion is a 180° sinusoidal angular displacement insertion profile of frequency 1 Hz, 2.5 Hz and 5 Hz, combined with continuous linear insertion at 10 mm/s. Tapping motion involves needle insertion in steps of 20 mm at 10 mm/s with pauses of 50 ms between each step.

The second experimental phase involves continuous needle insertion into the chicken liver (E_{liver}) which is suspended in a gel of elasticity E_1 (Experiment #6). The chicken liver is initially held in the gel using thin surgical strings. When the gel has solidified, the strings are removed. The needle used for this experiment is a 21G standard Chiba-tip biopsy needle with bevel angle of 30° (Fig. 2(b)).

Moreover, an additional study is performed to confirm the accuracy of the Aurora EM system. In this study, the Chiba-tip needle is inserted into gels of elasticities E_1 and E_2, and insertion speed is varied from 10 mm/s to 300 mm/s. The tip is tracked with both the stereoscopic cameras and the Aurora EM system. The results of this experiment are used to validate the accuracy of the EM system found from literature. Frantz *et al.* reported that translational and rotational accuracy of the system are 1.2 mm and 0.3°, respectively [20].

TABLE I

EXPERIMENTAL PLAN FOR INVESTIGATING 3D NEEDLE TIP DEFLECTION. INSERTION SPEED (V) OF 10 – 300 MM/S INDICATES CONTINUOUS LINEAR INSERTION AT 10 MM/S, 20 MM/S, 50 MM/S AND 300 MM/S, RESPECTIVELY. BEVEL ANGLE (β) OF 30° – 60° REPRESENTS NEEDLES WITH BEVEL ANGLES OF 30°, 45°AND 60°. GEL ELASTICITIES (E) ARE E_1=8.7 KPA, AND E_2=35.5 KPA. MOTION PROFILE (MP) INVESTIGATED ARE CONTINUOUS (CONT.), ROTATIONAL (ROT.) AND TAPPING (TAP.).

	System parameters			
Experiment	v (mm/s)	β (°)	E	MP
#1	10 – 300	30	E_1	Cont.
#2	10 – 300	30	E_2	Cont.
#3	10	30 – 60	E_1	Cont.
#4	10	30 – 60	E_2	Cont.
#5	10	30	E_1	Cont.; Rot. ; Tap.
#6	10 – 300	Chiba (30)	E_{liver}	Cont.
	10 – 300	Chiba (30)	E_1; E_2	Cont.

III. 3D NEEDLE TIP DEFLECTION

3D needle tip locations are reconstructed from 2D needle tip coordinates, which are obtained from stereo images using the 2D tip tracking algorithm.

A. 2D Tip Tracking

First, the tip coordinate ($[x_{i,k}, y_{i,k}]$) are extracted from each image using a 2D tip tracking algorithm. $[x_{(i,k)}, y_{(i,k)}]$ is the needle tip coordinate at time k, i is the camera reference frame, and k is given as the frame number.

The 2D tip tracking algorithm is developed based on Kalman filter, and the corner detector algorithm of Xiao *et al.* [21],[22],[23],[24]. Kalman filtering is used to estimate the needle tip coordinate in the next image frame $k+1$ ($[\hat{x}_{i,k+1}, \hat{y}_{i,k+1}]$). One cycle in the state estimation of the 2D needle tip coordinate is a standard Kalman filtering state estimation cycle [23]. The Kalman-predicted needle tip coordinates together with their associated prediction-covariance matrices are used to limit the search space of the corner detector algorithm. This prevents false tip detections due to other structures that are present in the image. The resolution of the stereoscopic cameras is 1024 by 768 pixels. Given a minimum image and process noise, the 2D tip tracking algorithm can locate the tip up to a sub-pixel resolution of a tenth of the camera pixel [22].

B. 3D Stereoscopic Reconstruction

3D needle tip locations are reconstructed using least squares error (LSE) estimation, applied on the correspondences of 2D needle tip coordinates [24]. The 3D measurement model can be derived from the perspective pinhole model of camera 1 and 2, respectively.

The estimated 3D needle tip location ($\hat{\mathbf{X}}_{3D,k}$) is calculated using LSE estimation as follows [24]:

$$\left.\begin{aligned}\hat{\mathbf{X}}_{3D,k} &= (\mathbf{H}_k^T \mathbf{C}_{\mathbf{z}_{4D}}^{-1} \mathbf{H}_k)^{-1} \mathbf{H}_k^T \mathbf{C}_{\mathbf{z}_{4D}}^{-1} \mathbf{z}_{4D,k}, \\ \mathbf{C}_{\hat{\mathbf{X}}_{3D,k}} &= (\mathbf{H}_k^T \mathbf{C}_{\mathbf{z}_{4D}}^{-1} \mathbf{H}_k)^{-1}.\end{aligned}\right\} \quad \text{LSE equations} \quad (1)$$

This solution is based on the inhomogeneous linear relation of $\mathbf{z}_{4D,k} = \mathbf{H}_k \mathbf{X}_{3D,k}$ that can be derived from the perspective projection of a pinhole camera model [24]. The extracted 2D tip coordinates ($[x_{i,k}, y_{i,k}]$) is incorporated in the 4×1 prediction vector ($\mathbf{z}_{4D,k}$), the 4×3 measurement matrix ($\mathbf{H}_k$), and the 4×4 noise covariance matrix ($\mathbf{C}_{\mathbf{z}_{4D}}$). $\hat{\mathbf{X}}_{3D,k}$ is a 3×1 vector of the estimated 3D needle tip location that is used to calculate the in-plane and out-of-plane deflection. Moreover, $\mathbf{C}_{\mathbf{z}_{4D}}$ and $\mathbf{C}_{\hat{\mathbf{X}}_{3D,k}}$ describes the measurement uncertainty in the 2D tip coordinates and 3D needle tip locations, respectively. In (1), it can also be deduced how the measurement uncertainty in the 2D tip coordinates propagates to the 3D needle tip locations.

In the experiment, we assume little prior knowledge of the 3D tip location, and $\hat{\mathbf{X}}_{3D,k}$ is initially set to the centre of a cubic working space. $\mathbf{C}_{\hat{\mathbf{X}}_{3D,k}}$ indicates that the 3D needle tip location can be estimated with an accuracy of 0.02 mm. This accuracy does not take into account the uncertainty that might occur due to the tolerance of camera calibration parameters.

IV. EXPERIMENTAL RESULTS

The experimental results of our first phase study are shown in Figs. 3 - 5, while the percentage changes in the maximum in-plane ($|\delta_{\text{in}}|$) and out-of-plane ($|\delta_{\text{out}}|$) deflection for all the six experimental studies are summarized in Table II.

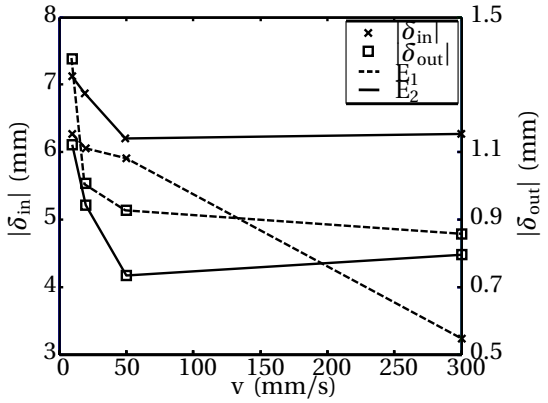

Fig. 3. Maximum in-plane ($|\delta_{in}|$) and maximum out-of-plane deflection ($|\delta_{out}|$) for variation in insertion velocity (v) and gel elasticity (E_1=8.7 kPa and E_2=35.5 kPa). In all experiments, β=30° and ϕ=1 mm. Mean standard deviation in $|\delta_{in}|$ and $|\delta_{out}|$ is 0.2 mm and 0.2 mm, respectively. *Experimental data points of the same gel elasticity are connected by straight lines. These lines are not meant to interpolate the data points, but provided for clarity.*

Experiments #1 and #2 :

Fig. 3 presents the effects of the variations in insertion velocity (v) and gel elasticity (E_1 and E_2) on $|\delta_{in}|$ and $|\delta_{out}|$. For gel elasticity E_1, the large portion of the drop in $|\delta_{in}|$ (45%) is observed when v increases from 50 mm/s to 300 mm/s (Fig. 3). For both gel elasticities (E_1 and E_2), an increase in v results in a drop in both $|\delta_{in}|$ and $|\delta_{out}|$ (Table II). Furthermore, the change in gel elasticity from E_2 to E_1 is noted to decrease $|\delta_{in}|$, and increase $|\delta_{out}|$.

Experiments #3 and #4 :

The effects of the variations in bevel angle (β) and gel elasticity (E_1 and E_2) on $|\delta_{in}|$ and $|\delta_{out}|$ are presented in Fig. 4. The variation in β from 30° to 60° decreases and increases $|\delta_{in}|$ and $|\delta_{out}|$, respectively (Table II). Moreover, the change in gel elasticity from E_2 to E_1 results in a decrease in $|\delta_{in}|$, and an increase in $|\delta_{out}|$.

Experiment #5 :

The effects of the variation in insertion profiles on $|\delta_{in}|$ and $|\delta_{out}|$ are shown in Fig. 5. The addition of 180° sinusoidal angular displacement reduces both $|\delta_{in}|$ and $|\delta_{out}|$. The increase in the frequency of sinusoidal angular displacement from 1 Hz to 5 Hz decreases $|\delta_{in}|$ and $|\delta_{out}|$ (Table II). Both tapping motion and the addition of 1 Hz sinusoidal angular displacement to continuous linear insertion have similar effects on $|\delta_{in}|$ and $|\delta_{out}|$ (Fig. 5).

Experiment #6 :

Figs. 6 and 7 present the results of our second phase study. In Fig. 6, the needle tip is tracked using both the stereoscopic cameras and the EM tracker. Gel elasticities are E_1 and E_2, and a Chiba-tip needle is inserted into the gels. For both gel elasticities (E_1 and E_2), it is observed that the variation in v from 10 mm/s to 300 mm/s decreases both $|\delta_{in}|$ and $|\delta_{out}|$ (Fig. 6). It is also noted that the maximum discrepancy between the two tracking methods is 0.7 mm, and it is observed for $|\delta_{in}|$ and gel elasticity E_2 (Fig. 6(b)). The experimental results noted during insertion into the chicken liver suspended in a gel of elasticity E_1 are shown in Fig. 7. The variation in v from 10 mm/s to 300 mm/s decreases $|\delta_{in}|$, and increases $|\delta_{out}|$ (Table II).

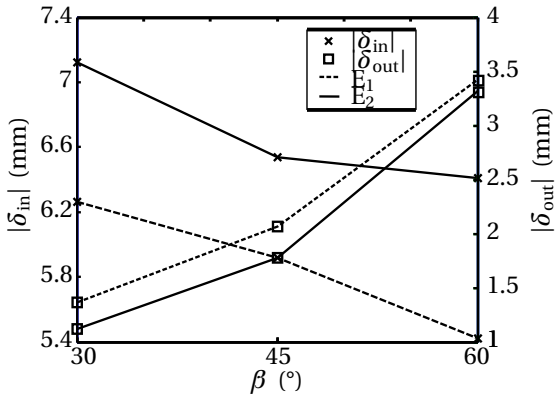

Fig. 4. Maximum in-plane ($|\delta_{in}|$) and maximum out-of-plane deflection ($|\delta_{out}|$) for variation in bevel angle (β) and gel elasticity (E_1=8.7 kPa and E_2=35.5 kPa). In all experiments, v=10 mm/s and ϕ=1 mm. Mean standard deviation in $|\delta_{in}|$ and $|\delta_{out}|$ is 0.2 mm and 0.1 mm, respectively. *Experimental data points of the same gel elasticity are connected by straight lines. These lines are not meant to interpolate the data points, but provided for clarity.*

V. Discussion and Future Work

Our result shows that the increase in v reduces both $|\delta_{in}|$ and $|\delta_{out}|$ (Fig. 3). The variation in v from 10 mm/s to 300 mm/s increases the needle linear momentum, and correspondingly the force required to cause needle bending. The increase in speed also results in smaller soft-tissue deformation and frictional force [25],[26]. Coupling of the increase in the needle linear momentum and the decrease in the frictional force results in the monotonic decrease in $|\delta_{in}|$ and $|\delta_{out}|$.

The increase in β from 30° to 60° results in a decrease in $|\delta_{in}|$, and an increase in $|\delta_{out}|$. The largest $|\delta_{out}|$ is 3.5 mm, and it is noted for β=60° and gel elasticity E_1 (Fig. 4). The trend noted for $|\delta_{in}|$ is consistent with the previous work by Misra *et al.* [27]. Using a mechanics-based model, they showed that $|\delta_{in}|$ was related to the geometry properties of the needle. i.e., $|\delta_{in}|$ increased as β decreased.

In our recent publication, 3D microscopic observations of gel rupture at the needle tip was shown to be narrow and long for a small β, and became wider and shorter for a large β [28]. This wide and short gel rupture for the large β provides a larger clearance for the tip to move

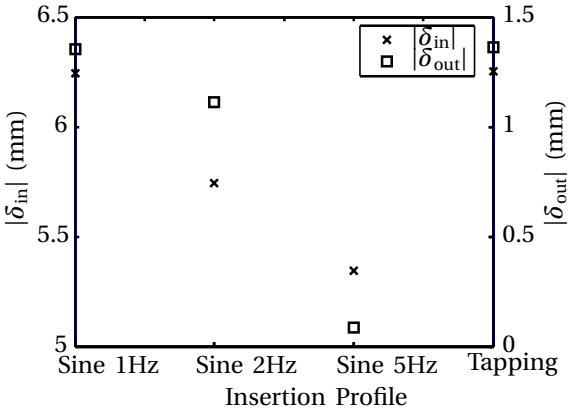

Fig. 5. Maximum in-plane ($|\delta_{in}|$) and maximum out-of-plane deflection ($|\delta_{out}|$) for rotational and tapping motion. In all experiments, E_1=8.7 kPa, v=10 mm/s, and ϕ=1 mm. In rotational motion, 1 Hz, 2 Hz, and 5 Hz of 180° sinusoidal angular displacement are added to a continuous linear insertion (Sine 1 Hz, Sine 2 Hz, and Sine 5 Hz, respectively). Mean standard deviation in $|\delta_{in}|$ and $|\delta_{out}|$ is 0.2 mm and 0.1 mm, respectively.

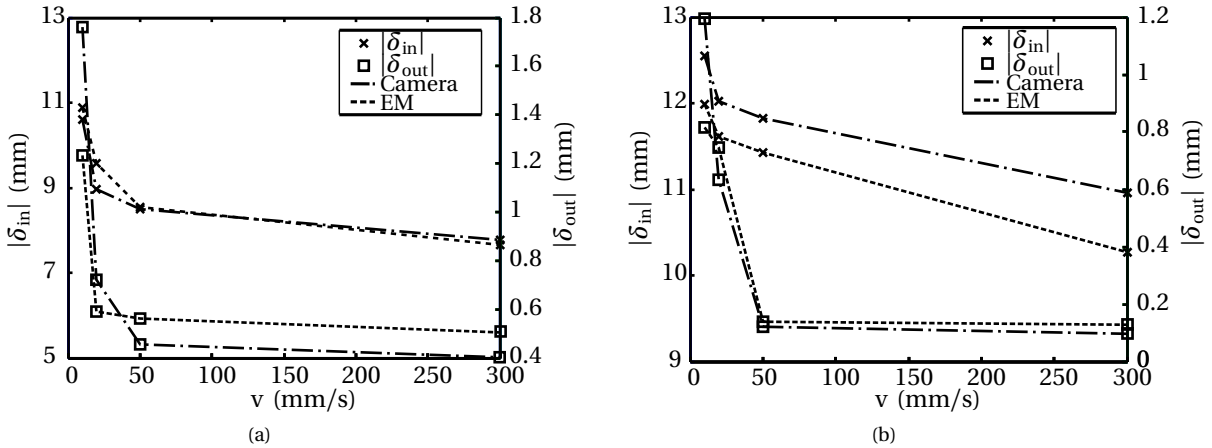

Fig. 6. Maximum in-plane ($|\delta_{in}|$) and maximum out-of-plane deflection ($|\delta_{out}|$) for variation in insertion velocity (v). A 21G Chiba-tip needle is inserted into a gel of elasticity: (a) E_1=8.7 kPa, and (b) E_2=35.5 kPa. The needle tip is tracked with the stereoscopic cameras and the electromagnetic (EM) tracker. For the stereoscopic cameras, mean standard deviation in $|\delta_{in}|$ and $|\delta_{out}|$ is 0.2 mm and 0.1 mm, respectively. On the other hand, for the EM tracker, mean standard deviation in $|\delta_{in}|$ and $|\delta_{out}|$ is 0.4 mm and 0.6 mm, respectively. *Experimental data points of the same tracking method are connected by straight lines. These lines are not meant to interpolate the data points, but provided for clarity.*

out-of-plane. Thus, $|\delta_{out}|$ increases as β increases (Fig. 4).

Moreover, for the variation in v and β, the change in gel elasticity from E_1 to E_2 is noted to increase $|\delta_{in}|$, and decrease $|\delta_{out}|$ (Figs. 3 and 4). The decrease in $|\delta_{out}|$ can be explained by considering the needle as a long thin cantilever beam. The weight of the needle results in a moment that deforms the needle in the direction perpendicular to the insertion direction (taken as positive out-of-plane moment). However, needle-gel interaction forces provide support during insertion, resulting in a moment that counters the positive out-of-plane moment. For gel elasticity E_2, the resultant positive out-of-plane moment will be less since its elasticity value is higher than E_1. Thus, $|\delta_{out}|$ is noted to be smaller for gel elasticity E_2 than for E_1.

The addition of rotational motion from 1 Hz to 5 Hz during continuous linear motion decreases both $|\delta_{in}|$ and $|\delta_{out}|$ (Fig. 5). Our results show that the increase in the frequency of rotational motion from 2 Hz to 5 Hz decreases both $|\delta_{in}|$ and $|\delta_{out}|$ by 10%. On the other hand, the increase in the frequency from 1 Hz to 2 Hz decreases $|\delta_{in}|$ and $|\delta_{out}|$ only by 2% (Fig. 5). However, fast needle rotation might cause tissue damage.

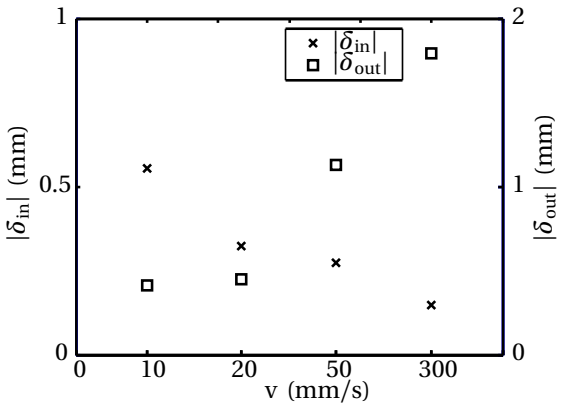

Fig. 7. Maximum in-plane ($|\delta_{in}|$) and maximum out-of-plane deflection ($|\delta_{out}|$) for continuous linear insertion into the chicken liver suspended in a gel of elasticity E_1. In all experiments, a 21G Chiba-tip needle is used. Experimental data points are for insertion speed of 10 mm/s, 20 mm/s, 50 mm/s and 300 mm/s, respectively. Mean standard deviation in $|\delta_{in}|$ and $|\delta_{out}|$ is 0.4 mm and 0.6 mm, respectively.

In Experiment #6, the diameter of Chiba-tip needle used is 21G (approximately 0.7 mm). Our results show that for both gel elasticities (E_1 and E_2), the variation in the insertion speed from 10 mm/s to 300 mm/s decreases both $|\delta_{in}|$ and $|\delta_{out}|$ (Fig. 6). When 1 mm diameter stainless-steel needle is used, similar trends in $|\delta_{in}|$ and $|\delta_{out}|$ are observed (Fig. 3). This shows that the effect of varying insertion speed on 3D needle deflection is consistent.

The maximum discrepancy noted between the two tracking methods is 0.7 mm (Fig. 6), and it is within the 1.2 mm error tolerance of the Aurora EM system [20]. Moreover, our results show that this discrepancy does not influence the trends noted in the experimental results (Figs. 3 and 6). The discrepancy is due to the use of metallic objects (i.e., needle stylet and cannula which are made from stainless-steel).

In the soft tissue experiment, a monotonic increase in $|\delta_{out}|$ is noted (Fig. 7). This might be due to the fact that the needle encounters the internal structure of the liver, or slips out-of-plane when it penetrates the outer capsule of the liver. Moreover, the cutting force is known to be significant during insertion into soft tissue [29]. This might contribute to the upward trend in $|\delta_{out}|$ during insertion into chicken liver.

The largest $|\delta_{in}|$ observed during insertion into the chicken liver is 0.6 mm (Fig. 7). On the other hand, the largest $|\delta_{in}|$ noted for a similar experiment using a homogeneous gel of elasticity E_1 is 10.9 mm (Fig. 6(a)). The significant difference (94%) between the largest $|\delta_{in}|$ noted during insertion into a homogenous gel of elasticity E_1 and the chicken liver is due to the small elasticity value of the chicken liver. The Young's modulus of the chicken liver is 2.6 kPa ± 1.9 kPa, while the elasticity value of E_1 is 8.7 kPa. Measurement of the elasticity value of the chicken liver is done using Virtual Touch™ Quantification installed on a Siemens Acuson S2000 ultrasound machine (Siemens

TABLE II

$|\delta_{\text{in}}|$ AND $|\delta_{\text{out}}|$ FOR THE SIX EXPERIMENTAL STUDIES (EXP). $\Uparrow \upsilon$ REPRESENTS AN INCREASE IN INSERTION VELOCITY FROM 10 MM/S TO 300 MM/S. $\Uparrow \beta$ REPRESENTS AN INCREASE IN BEVEL ANGLE FROM 30° TO 60°. $\Uparrow f$ REPRESENTS AN INCREASE IN THE ROTATIONAL MOTION FREQUENCY FROM 1 HZ TO 5 HZ. $E_2 \rightarrow E_1$ REPRESENTS A DECREASE IN GEL ELASTICITY FROM E_2 TO E_1. CONT AND ROT REPRESENTS CONTINUOUS AND ROTATIONAL INSERTION MOTION PROFILE, RESPECTIVELY. $\triangle$ AND ∇ REPRESENTS AN INCREASE AND A DECREASE IN PERCENTAGE, RESPECTIVELY. PERCENTAGE CHANGE IS CALCULATED AS $\% = \frac{\text{maximum } |\delta_{\text{in}}| - \text{minimum } |\delta_{\text{in}}|}{\text{minimum } |\delta_{\text{in}}|} \times 100$. A SIMILAR EQUATION APPLIES TO THE PERCENTAGE CHANGE IN $|\delta_{\text{out}}|$.

		E_1		E_2		E_1		E_2		E_1		E_{liver}	
		Exp #1		Exp #2		Exp #3		Exp #4		Exp #5		Exp #6	
		$\lvert\delta_{\text{in}}\rvert$	$\lvert\delta_{\text{out}}\rvert$	$\lvert\delta_{\text{in}}\rvert$	$\lvert\delta_{\text{out}}\rvert$	$\lvert\delta_{\text{in}}\rvert$	$\lvert\delta_{\text{out}}\rvert$	$\lvert\delta_{\text{in}}\rvert$	$\lvert\delta_{\text{out}}\rvert$	$\lvert\delta_{\text{in}}\rvert$	$\lvert\delta_{\text{out}}\rvert$	$\lvert\delta_{\text{in}}\rvert$	$\lvert\delta_{\text{out}}\rvert$
Cont	$\Uparrow \upsilon$	∇ 48%	∇ 42%	∇ 41%	∇ 27%							∇ 73%	$\triangle$ 366%
	$\Uparrow \beta$					∇ 13%	$\triangle$ 159%	∇ 10%	$\triangle$ 178%				
Rot	$\Uparrow f$									∇ 14%	∇ 93%		
	$E_2 \rightarrow E_1$	$\lvert\delta_{\text{in}}\rvert$: ∇ 47% $\lvert\delta_{\text{out}}\rvert$: $\triangle$ 15%				$\lvert\delta_{\text{in}}\rvert$: ∇ 12% $\lvert\delta_{\text{in}}\rvert$: $\triangle$ 14%							

AG, Erlangen, Germany).

An immediate extension of this study is an investigation into target motion during needle insertion. Experiments can be done by embedding a stiff target in gel or an EM sensor in biological tissue. Further, an investigation into 3D tip deflection during insertion into soft tissue of ranging elasticity will also be a valuable addition to this study.

In conclusion, the results of this study can be used to optimize needle design and insertion profile, and to develop an accurate model of needle-tissue interactions. Such a needle-tissue interaction model could aid the development of pre-operative plans in order to improve the accuracy of needle tip placement during the percutaneous procedures. Moreover, accounting both in-plane and out-of-plane deflection during needle insertion will further minimize needle targeting error. Subsequently, this will improve conclusiveness of the diagnosis and effectiveness of the treatment.

REFERENCES

[1] T. De Silva *et al.*, "Quantification of prostate deformation due to needle insertion during TRUS-guided biopsy: comparison of hand-held and mechanically stabilized systems," *Medical Physics*, vol. 38, no. 3, pp. 1718–1731, 2011.

[2] M. Meltsner *et al.*, "Observations on rotating needle insertions using a brachytherapy robot," *Physics in Medicine and Biology*, vol. 52, no. 19, pp. 6027–6037, 2007.

[3] O. Goksel *et al.*, "Modeling and simulation of flexible needles," *Medical Engineering & Physics*, vol. 31, no. 9, pp. 1069–1078, 2009.

[4] S. P. DiMaio and S. E. Salcudean, "Needle insertion modelling and simulation," in *Proc. IEEE Int. Conf. Robotics and Automation (ICRA), Washington, DC, USA*, 2002, pp. 2098–2105.

[5] G. Wan *et al.*, "Brachytherapy needle deflection evaluation and correction," *Medical Physics*, vol. 32, no. 4, pp. 902–909, 2005.

[6] A. M. Okamura *et al.*, "Force modeling for needle insertion into soft tissue," *IEEE Transactions on Biomedical Engineering*, vol. 51, pp. 1707–1716, Oct. 2004.

[7] H. Kataoka *et al.*, "Measurement of the tip and friction force acting on a needle during penetration," in *Proc. Int. Conf. Medical Image Computing and Computer-Assisted Intervention (MICCAI), London, UK*, 2002, pp. 216–223.

[8] N. Abolhassani *et al.*, "Control of soft tissue deformation during robotic needle insertion," *Minimally Invasive Therapy and Allied Technologies*, vol. 15, no. 3, pp. 165–176, 2006.

[9] G. Wan *et al.*, "Needle steering for 3D TRUS-guided robot-aided brachytherapy," in *Proc. Int. Congr. Exhib. Computer Assisted Radiology and Surgery (CARS), Chicago, USA*, 2004, p. 1325.

[10] D. Minhas *et al.*, "Modeling of needle steering via duty-cycled spinning," in *Proc. IEEE/EMBS Int. Conf. Engineering in Medicine and Biology Society (EMBC), Lyon, France*, 2007, pp. 2756–2759.

[11] H. Kataoka *et al.*, "A model for relations between needle deflection, force, and thickness on needle penetration," in *Proc. Int. Conf. Medical Image Computing and Computer-Assisted Intervention (MICCAI), Utrecht, The Netherlands*, 2001, pp. 966–974.

[12] M. Hochman and N. Friedman, "In vitro study of needle deflection: a linear insertion technique versus bidirectional rotation insertion technique," *Quintessence International*, vol. 31, no. 1, pp. 33–39, 2000.

[13] R. J. Webster *et al.*, "Design considerations for robotic needle steering," in *Proc. IEEE Int. Conf. Robotics and Automation (ICRA), Barcelona, Spain*, 2005, pp. 3588–3594.

[14] V. V. Karnik *et al.*, "Assessment of image registration accuracy in three-dimensional transrectal ultrasound guided prostate biopsy," *Medical Physics*, vol. 37, no. 2, pp. 802–813, 2010.

[15] P. Wust *et al.*, "Clinical and physical determinants for toxicity of 125-i seed prostate brachytherapy," *Radiotherapy and Oncology*, vol. 73, no. 1, pp. 39–48, 2004.

[16] M. J. Zelefsky *et al.*, "Improved conformality and decreased toxicity with intraoperative computer-optimized transperineal ultrasound-guided prostate brachytherapy," *International Journal of Radiation Oncology · Biology · Physics*, vol. 55, no. 4, pp. 956–963, 2003.

[17] Benninghoff, *Makroskopische Anatomie, Embryologie und Histologie des Menschen.*, 1st ed. Urban und Schwarzenberg, 1993.

[18] J. op den Buijs *et al.*, "Predicting target displacements using ultrasound elastography and finite element modeling," *IEEE Transactions on Biomedical Engineering*, vol. 58, pp. 3143–3155, Nov. 2011.

[19] T. K. Podder *et al.*, "Effects of velocity modulation during surgical needle insertion," in *Proc. IEEE/EMBS Int. Conf. Engineering in Medicine and Biology Society (EMBC), Shanghai, China*, 2005, pp. 5766–5770.

[20] D. Frantz *et al.*, "Accuracy assessment protocols for electromagnetic tracking system," *Physics in Medicine and Biology*, vol. 48, no. 14, pp. 2241–2251, 2003.

[21] C. H. Xiao and H. Yung, "Corner detector based on global and local curvature properties," *Optical Engineering*, vol. 47, no. 5, pp. 1–12, 2008.

[22] R. J. Roesthuis *et al.*, "Mechanics of needle-tissue interaction," in *Proc. IEEE/RSJ Int. Conf. Intelligent Robots and Systems (IROS), San Francisco, California, USA*, 2011, pp. 2557–2563.

[23] Y. Bar-Shalom and X. Rong Li, *Estimation and Tracking: Principles, Techniques, and Software*, 1st ed. Artech House, Inc., 1993.

[24] R. I. Hartley and A. Zisserman, *Multiple View Geometry in Computer Vision*, 2nd ed. Cambridge University Press, 2000.

[25] V. Lagerburg *et al.*, "Development of a tapping device: a new needle insertion method for prostate brachytherapy," *Physics in Medicine and Biology*, vol. 51, no. 4, pp. 891–902, 2006.

[26] R. Alterovitz *et al.*, "Needle insertion and radioactive seed implantation in human tissues: simulation and sensitivity analysis," in *Proc. IEEE Int. Conf. Robotics and Automation (ICRA), Taipei, Taiwan*, 2003, pp. 1793–1799.

[27] S. Misra *et al.*, "Mechanics of flexible needles robotically steered through soft tissue," *International Journal of Robotics Research*, vol. 29, no. 13, pp. 1640–1660, 2010.

[28] Y. R. J. van Veen *et al.*, "Macroscopic and microscopic observations of needle insertion into gels," *Proceedings of the Institute of Mechanical Engineering Part H, Journal of Engineering in Medicine*, 2012. *In Press.*

[29] C. Simone and A. M. Okamura, "Modeling of needle insertion forces for robot-assisted percutaneous therapy," in *Proc. IEEE Int. Conf. Robotics and Automation (ICRA), Washington, DC, USA*, 2002, pp. 2085–2091.